

A PROBABLE MILLI-PARSEC SUPERMASSIVE BINARY BLACK HOLE IN THE NEAREST QUASAR MRK 231

CHANG-SHUO YAN¹, YOUJUN LU^{1,†}, XINYU DAI², & QINGJUAN YU³

¹National Astronomical Observatories, Chinese Academy of Sciences, Beijing, 100012, China; [†]luyj@nao.cas.cn

²Homer L. Dodge Department of Physics and Astronomy, The University of Oklahoma, Norman OK, 73019, USA

³Kavli Institute for Astronomy and Astrophysics, Peking University, Beijing, 100871, China

Draft version July 25, 2018

ABSTRACT

Supermassive binary black holes (BBHs) are unavoidable products of galaxy mergers and are expected to exist in the cores of many quasars. Great effort has been made during the past several decades to search for BBHs among quasars; however, observational evidence for BBHs remains elusive and ambiguous, which is difficult to reconcile with theoretical expectations. In this paper, we show that the distinct optical-to-UV spectrum of Mrk 231 can be well interpreted as emission from accretion flows onto a BBH, with a semimajor axis of ~ 590 AU and an orbital period of ~ 1.2 year. The flat optical and UV continua are mainly emitted from a circumbinary disk and a mini-disk around the secondary black hole (BH), respectively; and the observed sharp drop off and flux deficit at $\lambda \sim 4000 - 2500\text{\AA}$ is due to a gap (or hole) opened by the secondary BH migrating within the circumbinary disk. If confirmed by future observations, this BBH will provide a unique laboratory to study the interplay between BBHs and accretion flows onto them. Our result also demonstrates a new method to find sub-parsec scale BBHs by searching for deficits in the optical-to-UV continuum among the spectra of quasars.

Subject headings: accretion, accretion discs - black hole physics - galaxies: active - galaxies: nuclei - galaxies: individual (Mrk 231) - quasars: supermassive black holes

1. INTRODUCTION

Supermassive binary black holes (BBHs) are natural products of the hierarchical mergers of galaxies in the Λ CDM cosmology and are expected to be abundant (e.g., Begelman et al. 1980; Yu 2002; Merritt & Milosavljević 2005), since many galaxies (if not all) are found to host a supermassive black hole (SMBH) at their centers (e.g., Magorrian et al. 1998; Kormendy & Ho 2013). Evidence has been accumulated for SMBH pairs in active galactic nuclei (AGNs) and quasars with perturbed galaxy morphologies or other merger features (e.g., Komossa et al. 2003; Liu et al. 2010; Comerford et al. 2011; Fu et al. 2012). These SMBH pairs will unavoidably evolve to closely bound BBHs with separations less than 1 pc. However, the evidence for BBHs at the sub-pc scale is still elusive (e.g., Popović 2012), which raises a challenge to our understanding of the BBH merger process and the formation and evolution of SMBHs and galaxies.

A number of BBH candidates in quasars have been proposed according to various spectral or other features, such as the double-peaked, asymmetric, or offset broad line emission (e.g., Boroson & Lauer 2009; Tsalmantza et al. 2011; Eracleous et al. 2012; Ju et al. 2013; Liu et al. 2014), the periodical variations (e.g., Valtonen et al. 2008; Graham et al. 2015), and etc.; however, most of those candidates are still difficult to be confirmed. Thus, it is of great importance to find other ways to select and identify BBHs in quasars. Recently, Gültekin & Miller (2012) proposed that the continuum emission from a BBH-disk accretion system, with unique observable signatures between 2000\AA and $2\mu\text{m}$ because of a gap or a hole in the inner part, can be used to diagnose BBHs (see Sesana et al. 2012; Roedig et al. 2014; Yan et al. 2014, but Farris et al. 2015). This method may be efficient in identifying BBHs since many AGNs and quasars have multi-wavelength observations and broad band spectra. Those previous investigations only focus on theoretical predictions, and

the present paper is the first attempt to apply this method to fit real observations.

In this paper, we report a BBH candidate in the core of Mrk 231, the nearest quasar with a redshift $z = 0.0422$, according to its unique optical-UV spectrum. In Section 2, we summarize the multi-wavelength spectrum of Mrk 231 and its distinctive spectral features comparing with normal quasars. The spectrum of Mrk 231 at the optical band is similar to the quasar composite spectrum; however, it drops dramatically at the wavelengths around 3000\AA and becomes flat again at $\lesssim 2500\text{\AA}$. This anomalous continuum is hard to be explained by normal extinction/absorption (Veilleux et al. 2013). We propose that the unique optical-to-UV spectrum of Mrk 231 can be explained by emission from a BBH accretion system, with which the drop of the continuum at $\lesssim 4000\text{\AA}$ is due to a gap or a hole opened by the secondary component of the BBH. In Section 3, we introduce a simple (triple-)disk model for the accretion onto a BBH system. Using this model, we fit the optical-to-UV continuum of Mrk 231 (Section 4) and constrain the orbital configuration of the BBH system and the associated physical parameters of the accretion process in Section 5. Discussions and conclusions are given in Sections 6 and 7.

2. MULTI-BAND OBSERVATIONS OF MRK 231

Mrk 231 is an ultraluminous infrared galaxy with a bright quasar-like nucleus. It is probably at the final stage of a merger of two galaxies as suggested by its disturbed morphology and the associated tidal features (Lipari & Macchetto 1994; Armus et al. 1994). The broadband spectrum of the Mrk 231 nucleus exhibits some extreme and surprising properties as follows.

First, the flux spectrum (F_λ) drops dramatically by a factor of ~ 10 at the near UV band (from wavelength $\lambda \sim 4000\text{\AA}$ to 2500\AA), while it is flat at $\lambda \sim 1000\text{\AA} - 2500\text{\AA}$ and at $\lambda \sim$

4000 Å–10000 Å. If this sharp drop off is due to extinction, it requires a large dust reddening of $A_V \sim 7$ mag at $\lambda \sim 2500 - 4000$ Å and a small dust reddening ~ 0.5 mag at < 2500 Å (Veilleux et al. 2013). Thus, an unusual complex geometric structure for the extinction material surrounding the disk must be designed (Veilleux et al. 2013; Leighly et al. 2014).

Second, Mrk 231 is an extremely powerful Fe II emitter as suggested by the spectrum on the blue side of H_α and on both sides of H_β . Such a high level of optical Fe line emission suggests a significant amount of Fe line emission at the UV band; however, it is not visible in the observed UV spectrum (Veilleux et al. 2013; Leighly et al. 2014).

Third, a number of broad low-ionization absorption line systems, such as Na I D, Ca II, Mg II, Mg I, and Fe II, have been identified in the optical-to-UV spectrum, which suggests that Mrk 231 should be an Fe low-ionization broad absorption line quasar (FeLoBAL) (Veilleux et al. 2013). However, the expected corresponding absorption features at the UV and FUV bands are not evident.

Fourth, the hard X-ray emission of Mrk 231 is extremely weak. The intrinsic, absorption corrected, X-ray luminosity at 2–10 keV is $L_{2-10\text{keV}} \sim 3.8 \times 10^{42} \text{ erg s}^{-1}$, and the ratio of $L_{2-10\text{keV}}$ to the bolometric luminosity (inferred from the optical luminosity) is only ~ 0.0003 (Saez et al. 2012; Teng et al. 2014), almost two orders of magnitude smaller than the typical value (~ 0.03) of a quasar with a similar bolometric luminosity (Hopkins et al. 2007).

Below we show that the above first feature, the anomalous UV continuum, is a distinct prediction of a BBH–disk accretion system as shown in Figure 1. The last three features, commonly interpreted under the context of complicated outflows with absorptions, can be also accommodated under the framework of the BBH–disk accretion, e.g., the wind features are consistent with the Fe absorption features of a typical FeLoBAL, and Mrk 231’s intrinsic X-ray weakness is also a natural consequence of a BBH–disk accretion system with a small mass ratio.

3. OPTICAL-TO-UV CONTINUUM FROM A BINARY BLACK HOLE—(TRIPLE-)DISK ACCRETION SYSTEM

Considering a BBH system resulting from a gas rich merger, the BBH is probably surrounded by a circumbinary disk, and each of the two SMBHs is associated with a mini-disk (see Fig. 1). In between the circumbinary disk and the inner mini-disks, a gap (or hole) is opened by the secondary SMBH, which is probably the most distinct feature of a BBH–disk accretion system, in analogy to a system in which a gap or hole is opened by a planet migrating in the planetary disk around a star (Lin et al. 1996; Quanz et al. 2013). This type of geometric configurations for the BBH–disk accretion systems has been revealed by many numerical simulations and analysis (Artymowicz & Lubow 1996; Dorazio et al. 2013; Hayasaki et al. 2008; Escala et al. 2005; Cuadra et al. 2009; Roedig et al. 2014; Farris et al. 2014).¹ The continuum emission from disk accretion onto a BBH may be much more complicated than that from disk accretion onto a single SMBH, since the dynamical interaction between the BBH and the accretion flow onto it changes the disk structure (Gültekin & Miller 2012; Sesana et al. 2012;

¹ The width of the gap (or hole) is roughly determined by, but could be somewhat larger than, the Hill radius R_H . However, set a slightly large gap size, e.g., $1.2R_H$, does not affect the results presented in this paper significantly.

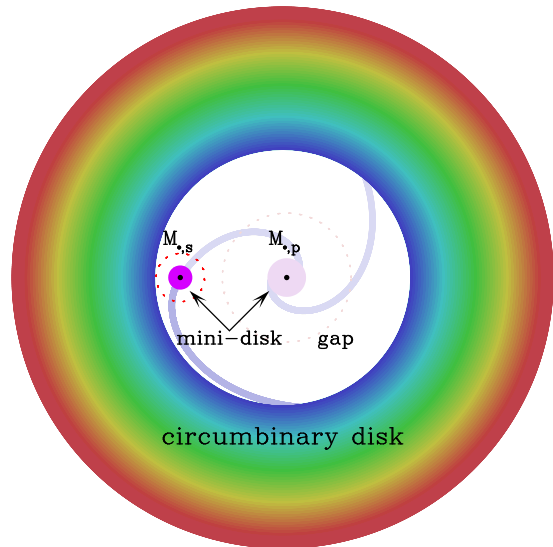


FIG. 1.— Schematic diagram for a BBH–disk accretion system. The BBH is assumed to be on circular orbits with a semimajor axis of a_{BBH} , and the masses of the primary and secondary components are $M_{\bullet,p}$ and $M_{\bullet,s}$, respectively. The BBH is surrounded by a circumbinary disk, connecting with the mini-disk around each component of the BBH by streams. In between the circumbinary disk and the inner mini-disks, a gap or hole is opened by the secondary SMBH (Artymowicz & Lubow 1996; Dorazio et al. 2013; Farris et al. 2014). The width of the gap (or hole) is roughly determined by the Hill radius $R_H [\sim a_{\text{BBH}}(M_{\bullet,s}/3M_{\bullet,p})^{1/3} \simeq 0.69q^{1/3}a_{\text{BBH}}]$, where q is the mass ratio, and the inner boundary of the circumbinary disk can be approximated as $r_{\text{in},c} \sim a_{\text{BBH}}/(1+q) + R_H$. The outer boundary of the mini-disk surrounding the secondary SMBH ($r_{\text{out},s}$) is assumed to be a fraction ($f_{r,s}$) of the mean Roche radius, $R_{\text{RL}}(q) \simeq 0.49a_{\text{BBH}}q^{2/3}/[0.6q^{2/3} + \ln(1 + q^{1/2})]$ (Eggleton 1983), i.e., $r_{\text{out},s} = f_{r,s}R_{\text{RL}}(q)$, considering that the mini-disk may not fill the whole Roche lobe (the red dashed circle). For BBHs with mass ratios roughly in the range from a few percent to 0.25, the accretion onto the secondary SMBH and consequently its emission dominates, compared with that from the mini-disk around the primary BH (Roedig et al. 2012; Farris et al. 2014).

Rafikov 2013; Roedig et al. 2014; Yan et al. 2014; Farris et al. 2015). Nevertheless, we adopt a simple model to approximate the continuum emission from a BBH–disk accretion system as the combination of the emissions from an outer circumbinary disk and an inner mini-disk around the secondary SMBH, each approximated by multicolor black body radiation in the standard thin disk model (Shakura & Sunyaev 1973; Novikov & Thorne 1973). The emission from the mini-disk around the primary SMBH is insignificant for a BBH system with a small mass ratio (roughly in the range of a few percent to 0.25) due to its low accretion rate as suggested by the state of the art numerical simulations (Roedig et al. 2012; Farris et al. 2014), thus its emission can be neglected. Our analysis suggests that a large q cannot lead to a good fit to the observations.

3.1. Emission from the circumbinary disk

We choose a standard thin disk to approximate the temperature profile of the circumbinary disk. The structure and spectral energy distribution (SED) of the circumbinary disk may be different from that of a standard thin disk, especially at the region close to the inner edge, since the torque raised by the central BBH may lead to gas accumulation there. In this region, the circumbinary disk is somewhat hotter than the corresponding region of a standard thin disk with the same accretion rate and total SMBH mass ($M_{\bullet,p} + M_{\bullet,s}$) (e.g., Rafikov 2013). We neglect this slight difference for now and will discuss this in the Appendix.

3.2. Emission from the inner mini-disk associated with the secondary SMBH

We assume that the emission from the inner mini-disks is dominated by that from the mini-disk around the secondary SMBH, and the emission from a mini-disk can also be approximated by that from a standard thin disk with the same extent, accretion rate, and SMBH mass. The accretion onto each of the two SMBHs may be highly variable (Roedig et al. 2012; Hayasaki et al. 2008), and the temperature structure of each of the two mini-disks may be affected by the torque from the other SMBH component, the outer circumbinary disk (Farris et al. 2015), and the infalling stream. We ignore those complications in the fitting and will discuss the related effects in Appendix.

In the standard thin accretion disk model, the emission from an annulus $r - dr/2 \rightarrow r + dr/2$ of the disk is approximated by a black body radiation with an effective temperature of

$$T_{\text{eff}}(r) = \left[\frac{3GM_{\bullet}\dot{M}_{\text{acc}}}{8\pi\sigma_{\text{B}}r^3} \left(1 - \sqrt{\frac{r_{\text{in}}}{r}} \right) \right]^{1/4}, \quad (1)$$

where G is the gravitation constant, σ_{B} is the Stefan-Boltzmann constant, \dot{M}_{acc} is the accretion rate of the SMBH, and r_{in} is the radius of the disk's inner edge. For the circumbinary disk, $r_{\text{in,c}} = a_{\text{BBH}}/(1+q) + R_{\text{H}}$; for the mini-disk around the secondary SMBH, $r_{\text{in,c}} \sim 3.5GM_{\bullet,\text{s}}/c^2 = 3.5r_{\text{g,s}}$, assuming a radiative efficiency $\epsilon \simeq 0.1$ (correspondingly an SMBH spin of $\simeq 0.67$; Yu & Lu 2008; Shankar et al. 2013). Here c is the speed of light. We can then obtain the continuum emission for either the circumbinary disk or the mini-disk around the secondary SMBH as

$$F_{\lambda} = \int_{r_{\text{in}}}^{r_{\text{out}}} \frac{2\pi r}{D_1^2} \frac{2hc^2 \cos i / \lambda^5}{\exp[hc/\lambda k_{\text{B}}T_{\text{eff}}(r)] - 1} dr, \quad (2)$$

where D_1 is the luminosity distance of Mrk 231, h is the Planck constant, k_{B} the Boltzmann constant, i the inclination angle, $r_{\text{out}} = 10^5 r_{\text{in,c}}$ and $f_{\text{r,s}}R_{\text{RL}}(q)$ for the circumbinary disk and the mini-disk, respectively. Here we simply assume $\cos i = 0.8$, the mean value for type 1 quasars. We find that a slight change of $\cos i$ does not affect our results significantly.

3.3. Pseudo-continuum from Fe emission lines

It has been shown that there are extremely strong Fe II emission lines in the optical spectrum of Mrk 231. Thousands of Fe emission lines from the broad line emission region blending together can form a pseudo-continuum. Therefore, the Fe emission must be included when fitting the SED of Mrk 231. We use the template-fitting method introduced by Phillips (1977), probably a standard practice, to treat the Fe emission in Mrk 231, in which the Fe spectrum of the narrow-line Seyfert 1 galaxy IZw 1 is used to construct an Fe II template. In the UV band, we adopt the Fe template of Vestergaard & Wilkes (2001). In the optical band, the Fe template is constructed according to the list of the Fe lines for I Zw 1 given in Véron-Cetty et al. (2004). We combine the UV and optical Fe templates to form a single template, convolve it by a Gaussian function with a width of $\text{FWHM}_{\text{conv}}$, and scale it by a factor of A_{s} to match the observations. The total flux of the Fe emission, I_{Fe} , is equal to A_{s} multiplied by the total flux of the template; the FWHM of the Fe lines can be expressed as $\text{FWHM}_{\text{Fe}} = \sqrt{\text{FWHM}_{\text{IZw1}}^2 + \text{FWHM}_{\text{conv}}^2}$. In the above algorithm, we assume that the Fe emissions in

the UV and optical bands have the same width and there is no shift between the redshifts of the UV and the optical lines. We also assume that the ratio of the UV Fe flux to the optical Fe flux is fixed to be the same as that of I Zw 1. A detailed dynamical model for the broadening and the shift of individual Fe emission lines is beyond the scope of our paper.

We have also further checked the validity of adopting the Fe template of IZw 1 by using a CLOUDY (Ferland et al. 2013) model, with the best fit continuum of Mrk 231 obtained below as the input intrinsic continuum. We find that the total flux of the UV Fe emission ($I_{\text{Fe,UV}}$) to the total flux of the optical Fe emission ($I_{\text{Fe,opt}}$) generated from the CLOUDY model (~ 3) is similar to that of IZw 1 if the ionization parameter is sufficiently small (~ 0.001). A small ionization parameter is compatible with the best-fit parameters of the BBH-disk accretion system, since the broad line emission region is bound to the primary SMBH, much more massive than the secondary SMBH, while the ionizing photons are provided by the mini-disk around the secondary SMBH. If $I_{\text{Fe,UV}}/I_{\text{Fe,opt}}$ is substantially smaller than that of IZw 1, then the FeLoBAL feature in Mrk 231 would be much less significant than that shown in Figures 3 and 7.

4. THE OPTICAL-TO-UV SPECTRUM OF MRK 231

The observed broadband spectrum of Mrk 231 is first shifted to the rest frame and then corrected for the Galactic extinction [$E(B-V) = 0.02213$], and the results are shown in Figure 2. A number of fitting windows are chosen in order to avoid those strong emission or absorption lines, such as $\text{H}\alpha$, $\text{H}\beta$, O III , $\text{Ly}\alpha$, and Na I D , which is the commonly adopted way to perform the continuum or SED fitting. The fitting windows adopted are 1140-1152, 1260-1300, 1340-1400, 1500-1650, 1860-2000, 3090-3145, 3740-3800, 4400-4700, 5080-5600, 6060-6350, and 6750-6850Å. A more complicated model may be developed by fitting each of the emission lines with one or more Gaussian components and each of the absorption lines with Voigt profile or Gauss-Hermit expansions; however, these lines will not affect the overall shape of the continuum, the focus of this paper, and thus we choose to simplify the presentation by not involving fittings to those emission and absorption lines. The wavelength range 3800-4400Å is also excluded because of the contamination from the high-order Balmer lines. The wavelength range from 2000 to 3000Å is excluded to avoid the uncertainties in modeling strong Fe absorption lines as indicated by the FeLoBAL signatures found in the optical band.

5. MCMC FITTING RESULTS

We use the Markov Chain Monte Carlo (MCMC) method to obtain the best fit to the observational data in the above fitting windows and constrain the model parameters. The parameters included in the continuum model are the total mass (M_{\bullet}), mass ratio (q), semimajor axis (a_{BBH}) of the BBH, the Eddington ratios of the outer circumbinary disk ($f_{\text{Edd,c}}$) and the inner mini-disk ($f_{\text{Edd,s}}$), the ratio of the outer boundary of the inner mini-disk to the mean Roche radius ($f_{\text{r,s}}$), the scale factor A_{s} and convolution width $\text{FWHM}_{\text{conv}}$ of the Fe emission lines, and the extinction $E_{\text{B-V}}$ due to the interstellar medium in Mrk 231. Here the Eddington ratio is defined as the ratio of the accretion rate of the circumbinary disk $\dot{M}_{\text{acc,c}}$ (or the secondary mini-disk $\dot{M}_{\text{acc,s}}$) to the accretion rate \dot{M}_{Edd} set by the Eddington limit (assuming $\epsilon = 0.1$), i.e., $f_{\text{Edd,c}} = \dot{M}_{\text{acc,c}}/\dot{M}_{\text{Edd}}(M_{\bullet}) = \epsilon\dot{M}_{\text{acc,c}}c^2/L_{\text{Edd}}(M_{\bullet})$,

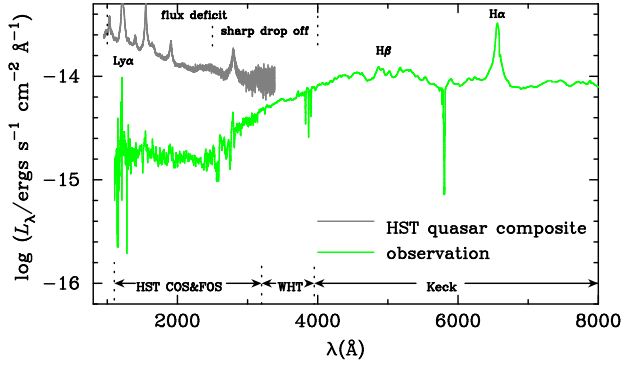


FIG. 2.— The optical-to-UV spectrum of Mrk231. The green curve represents the UV observations by the COS and FOS on board the HST (archive data; Veilleux et al. 2013; Smith et al. 1995), the observations by the William Herschel Telescope (WHT) and Keck telescope (Leighly et al. 2014). The wavelength ranges for those different observations are marked at the bottom of the figure. The FOS data is scaled up by a factor of 2 to match the COS data (see Veilleux et al. 2013). The grey curve represents the HST composite spectrum of quasars (Zheng et al. 1997). The continuum shows a sharp drop off at $\lambda \sim 4000 - 2500\text{\AA}$ and deficit of flux at $\lambda \sim 4000 - 1000\text{\AA}$. The locations of the emission lines $H\alpha$, $H\beta$, and $Ly\alpha$ are also marked in the figure.

$f_{\text{Edd},s} = \dot{M}_{\text{acc},s}/\dot{M}_{\text{Edd}}(M_{\bullet,s}) = \epsilon \dot{M}_{\text{acc},s} c^2 / L_{\text{Edd}}(M_{\bullet,s})$, $L_{\text{Edd}}(M_{\bullet}) = 1.3 \times 10^{46} \text{erg s}^{-1} (M_{\bullet}/10^8 M_{\odot})$, and $L_{\text{Edd}}(M_{\bullet,s}) = 1.3 \times 10^{46} \text{erg s}^{-1} (M_{\bullet,s}/10^8 M_{\odot})$. We first adopt those nine parameters (M_{\bullet} , q , a_{BBH} , $f_{\text{Edd},c}$, $f_{\text{Edd},s}$, $f_{r,s}$, A_s , $\text{FWHM}_{\text{conv}}$, E_{B-V}) to fit the spectrum and obtain the best fit, and then fix the two parameters A_s and $\text{FWHM}_{\text{conv}}$ ($\sim 3000 \text{km s}^{-1}$) at their best-fit values and obtain constraints on the other seven parameters (M_{\bullet} , q , a_{BBH} , $f_{\text{Edd},c}$, $f_{\text{Edd},s}$, $f_{r,s}$, E_{B-V}). In the fitting, we adopt an extinction curve for SMC according to (Pei 1992);² the Eddington ratios for the outer circumbinary disk and the inner mini-disk are assumed to be in the range from 0.1 to 1, since the standard thin disk model may be invalid if the Eddington ratio is substantially smaller than 0.1.

The top panel of Figure 3 shows the best-fit model to the continuum emission from the BBH-disk accretion system. The overall shape of the observed continuum can be reproduced by the BBH-disk accretion model. The best fit parameters are $M_{\bullet} = 1.5 \times 10^8 M_{\odot}$, $q = 0.026$, $f_{\text{Edd},c} = 0.5$, $f_{\text{Edd},s} = 0.6$, $a_{\text{BBH}} = 590 \text{AU} = 2.9 \text{mpc}$, and $f_{r,s} = 0.11$, respectively.³ According to the best-fit model, the circumbinary disk dominates the emission of Mrk231 in the optical band; the mini-disk dominates the FUV emission; the sharp drop off at $4000 - 2500\text{\AA}$ is mainly due to the cut off of the circumbinary disk and the gap (or hole) opened by the secondary SMBH, but not an extremely high extinction (see the top panel of Figure 3). It is also not a necessity to have different extinctions in different bands to explain the sharp drop off.

The second panel of Figure 3 also shows the best fit to the

² We have checked that choosing a different extinction curve (e.g., the one for LMC) does not qualitatively affect our results.

³ Note that the best fit value of $f_{\text{Edd},s} = 0.6$ means that the secondary SMBH accretes via a rate close to the Eddington limit. The numerical simulations suggest that the accretion rate onto the primary SMBH is smaller than that onto the secondary SMBH for a BBH-disk accretion system with a mass ratio of a few to 25 percent (e.g., Farris et al. 2014). For the BBH system that best fits the continuum, the accretion rate of the primary disk should be $\lesssim 0.01$, which is via the advection dominated accretion flow (ADAF) mode (Esin et al. 1997) and radiatively extremely inefficient, and thus its emission can be neglected. This validates the omission of the primary disk emission in the fitting.

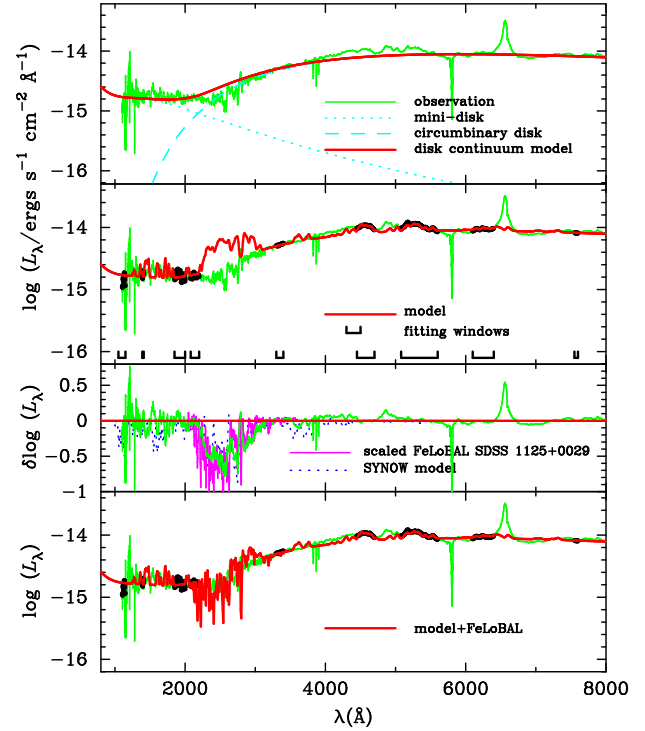


FIG. 3.— The optical-to-UV spectrum of Mrk231 and the model spectrum. From top to bottom, the first panel: the green curve represents the observations as that in Figure 2. The red curve represents the best-fit model for the continuum emission from the BBH-disk accretion system, a combination of the continuum emissions from the circumbinary disk (cyan dashed line) and the mini-disk around the secondary SMBH (cyan dotted line). The second panel: the green curve represents the observational spectrum of Mrk231. The red curve represents the best-fit continuum spectrum, a combination of the continuum emissions from the circumbinary disk, the mini-disk around the secondary SMBH, and the pseudo continuum by Fe emissions. The third panel: the green curve represents the residuals of the best fit continuum to the observations. The blue dotted curve represents the Fe absorption obtained from a model using SYNOW code, and the magenta solid curve represents the FeLoBAL absorption of SDSS 1125+0029 scaled by a factor of 1.6. The fourth panel: the red curve represents the model spectrum by adding the pseudo-continuum due to numerous Fe emission lines and including the contribution from the FeLoBAL absorption. The black points represent the observational data in those windows adopted in the continuum fitting as marked in this panel.

continuum emission of Mrk231, which includes not only the continuum emission from the circumbinary disk and the mini-disk around the secondary SMBH, but also the pseudo continuum from numerous Fe emission lines. The Fe emission of Mrk231 in the optical band is extremely high, and consequently the Fe emission in the UV band is likely to be high, too. In the observed UV spectrum, however, there appear no strong Fe emission lines (Veilleux et al. 2013; Leighly et al. 2014). Mrk231 is an FeLoBAL and should have very strong Fe absorptions in the UV band as indicated by the optical absorption lines, such as Na I D , but there appear no very strong Fe absorption lines in the observed UV spectrum. The reason is that the Fe absorption dominates over the Fe emission in this band as detailed below.

The third panel of Figure 3 shows the residuals of the model spectrum at $2000-3200\text{\AA}$ which reveals strong Fe absorption lines. These Fe absorption features are quite similar to a 1.6-time scale up of the FeLoBAL absorption features of SDSS 1125+0029 shown in Figure 4a of Hall et al. (2002, the magenta curve), of which no observation at $\lesssim 2000\text{\AA}$ is available. As an illustration, we further use the SYNOW code

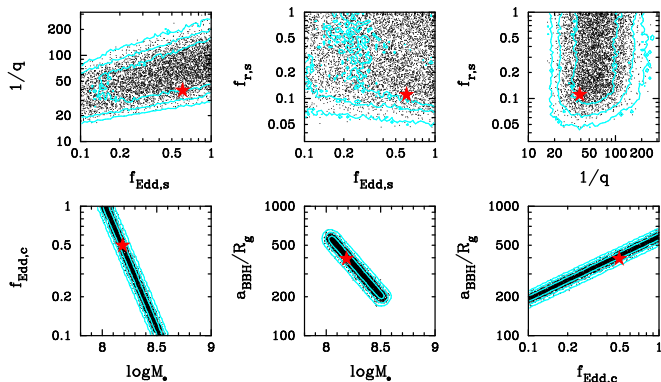


FIG. 4.— Two-dimensional probability contours for different parameters of the BBH. The red stars represent the best-fit parameter values. Only 50,000 points (black) out of 50,000,000 simulations are plotted. The cyan curves represent 1-, 2-, and 3 σ confidence contours from the inside to the outside, respectively.

(Branch et al. 2002), a fast parameterized synthetic-spectrum code, to generate a spectrum for the absorption features in the NUV band for Mrk 231. We assume that only the wind that covers the surface of the disk facing toward distant observers contributes to the absorption because of the optically thick disk, and this wind may launch at the inner edge of the circumbinary disk and/or from the mini-disk. For simplicity, we consider three species, i.e., Fe I, Fe II, and Mg II, and assume a temperature of 10000K, minimum velocity $v_{\min} = 1000 \text{ km s}^{-1}$, and maximum velocity $v_{\max} = 8000 \text{ km s}^{-1}$. The maximum velocity is on the same order of the escape velocity at a_{BBH} . The model absorption spectrum is shown in the bottom panel of Figure 3. It appears that the main absorption features seen in the residuals can be roughly modeled, though there are still some discrepancies in details. In the bottom panel of Figure 3, the model spectrum (red curve) is a combination of the best fit to the continuum and a 1.6-time scale up of the FeLoBAL absorption feature of SDSS 1125+0029 (cyan line in Fig. 3), which appears to match the observations well.

Figures 4 and 5 show the two-dimensional probability contours and one-dimensional marginalized probability distributions for the model parameters obtained from the MCMC fitting, respectively. The parameters M_{\bullet} , f_{Edd} , and a_{BBH} mainly determine the emission from the circumbinary disk and they are strongly degenerate with each other. If one of them could be determined by an independent method, the constraints on the other two would be significantly improved. The emission from the mini-disk around the secondary SMBH is determined by q , $f_{\text{Edd},s}$, and $f_{r,s}$, for which q and $f_{\text{Edd},s}$ are also degenerate with each other. The constraints on these three parameters can be substantially improved if observations at EUV (e.g., $\lesssim 1000\text{\AA}$) are available. According to the marginalized one-dimensional probability distribution for each parameter shown in Figure 5 by the standard MCMC technique, we have the peak values of the model parameters as $\log(M_{\bullet}/M_{\odot}) = 8.3^{+0.2}_{-0.2}$, $\log q = -1.8^{+0.2}_{-0.2}$, $\log f_{\text{Edd},c} = -0.5^{+0.4}_{-0.3}$, $\log f_{\text{Edd},s} = -0.4^{+0.3}_{-0.3}$, $\log(a_{\text{BBH}}/R_g) = 2.5^{+0.2}_{-0.2}$ (here $R_g = GM_{\bullet}/c^2$), $\log f_{r,s} = -0.5^{+0.4}_{-0.4}$, $E_{\text{B-V}} = 0.10^{+0.03}_{-0.03}$, and the orbital period $\simeq 1.2^{+0.2}_{-0.1}$ yr. Note these values for the model parameters are somewhat different from those from the best fit with minimum χ^2 -value.

The X-ray emission of AGNs and quasars is normally emitted from a corona structure above the inner disk area in

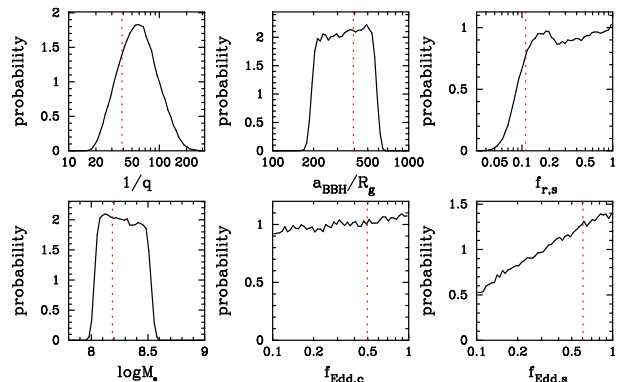


FIG. 5.— One-dimensional probability distributions of different parameters of the BBH. The red dotted vertical line in each panel represents the value of the best fit adopted in Figs. 2 and 3 to produce the model spectrum.

the standard disk–corona model (Haardt & Maraschi 1993; Dai et al. 2010). Here in Mrk 231, the outer circumbinary disk is truncated at a radius substantially larger than several hundreds of the Schwarzschild radius of the primary SMBH, for which the disk is too cold and a corona probably cannot be established above it to emit X-rays significantly. Therefore, the X-ray emission can only arise from the mini-disk or its associated corona around the secondary SMBH in the BBH–disk accretion model. Since the secondary SMBH is smaller than the primary one by a factor of $\sim 1/q \sim 38$, it is almost guaranteed that the X-ray emission from this system is much weaker than that from a single SMBH–disk accretion system with an SMBH mass of $M_{\bullet,p} + M_{\bullet,s}$ and an accretion rate of $f_{\text{Edd},c}M_{\bullet,\text{Edd},c}$ (or $f_{\text{Edd},s}M_{\bullet,\text{Edd},c}$). The best fit suggests that the observed X-ray luminosity of Mrk 231 in the 2–10 keV band is about 1% of the bolometric luminosity from the mini-disk, which is well consistent with those for normal AGNs and quasars (Hopkins et al. 2007). This solves the mystery of the intrinsic X-ray weakness of Mrk 231.

6. MODEL IMPLICATION AND DISCUSSIONS

According to the model fits, the intrinsic continuum and SED of Mrk 231 is significantly different from the canonical ones of normal quasars. The deficit of intrinsic UV emission will lead to substantially weaker broad line emissions compared with those of normal quasars. However, a number of broad emission lines, such as H_{α} , H_{β} , are evident in the optical spectrum of Mrk 231. The ratio of the H_{α} flux to the H_{β} flux is roughly 3, consistent with those of normal quasars. Here we check whether the total number of ionizing photons emitted by the central source is large enough to balance the total number of recombinations occurred in the broad line region. The total number of H_{β} photons is directly related to the number of ionizing photons as

$$L_{\text{H}\beta} = \frac{\Omega}{4\pi} \frac{\alpha_{\text{H}\beta}^{\text{eff}}(\text{H}^0, T)}{\alpha_{\text{B}}^{\text{eff}}(\text{H}^0, T)} h\nu_{\text{H}\beta} \int_{\nu_0}^{\infty} \frac{L_{\nu}}{h\nu} d\nu, \text{ where } \Omega/4\pi \text{ is the covering factor, } \alpha_{\text{H}\beta}^{\text{eff}}/\alpha_{\text{B}}^{\text{eff}} \sim 1/8.5 \text{ is the number of } \text{H}_{\beta} \text{ photons produced per hydrogen recombination, and } \nu_0 = c/912\text{\AA}, \nu_{\text{H}\beta} = c/4861\text{\AA} \text{ (Osterbrock \& Ferland 2006). Subtracting the best-fit continuum from the observed spectrum from } 4700\text{\AA} \text{ to } 5800\text{\AA}, \text{ we obtain } \text{H}_{\beta} \text{ luminosity by integrating the residual spectrum. Using the above equation, we find } \Omega/4\pi \sim 0.29, \text{ which is fully consistent with the typical range of } \Omega \text{ for AGNs/quasars and suggests that the ionizing photon emission from the mini-disk around the secondary SMBH is sufficient to produce the optical broad emission lines, such as}$$

$H\alpha$ and $H\beta$.

The inclination angle of the disk in Mrk 231 could be larger, e.g., $\cos i \sim 0.5$, since Mrk 231 is an FeLoBAL (though not a normal FeLoBAL in the BBH–disk accretion scenario) and FeLoBALs were suggested to have a larger i and a smaller $\cos i$ (Goodrich & Miller 2005). By alternatively setting $\cos i = 0.5$, the best fit obtained from the MCMC fitting suggests $\log(M_{\bullet}/M_{\odot}) = 8.5_{-0.2}^{+0.2}$, $\log q = -1.9_{-0.2}^{+0.2}$, $\log f_{\text{Edd,c}} = -0.5_{-0.4}^{+0.3}$, $\log f_{\text{Edd,s}} = -0.3_{-0.2}^{+0.2}$, $\log(a_{\text{BBH}}/R_{\text{g}}) = 2.5_{-0.2}^{+0.2}$, $\log f_{\text{r,s}} = -0.5_{-0.3}^{+0.3}$, and $E_{\text{B-V}} = 0.07_{-0.02}^{+0.02}$. With this BBH configuration, the orbital period is $1.6_{-0.2}^{+0.3}$ year and $\Omega/4\pi \simeq 0.5$. It appears that the results are qualitatively consistent with those obtained by assuming $\cos i = 0.8$. By relaxing the inclination angle as a free parameter, we find that our results are not affected significantly.

Numerical simulations suggest that the continuum emission from a BBH–disk accretion system may vary periodically due to the change of the material infalling rate from the circumbinary disk to the inner mini-disk(s) (e.g., Hayasaki et al. 2008), though the variation for those systems with small mass ratios (less than a few percent) may not be significant (e.g., Farris et al. 2014). Several UV observations of Mrk 231 have been obtained by *Hubble Space Telescope* (HST) over the years. The UV continuum of the HST COS observations by Veilleux et al. (2013) is roughly consistent with the HST G160H observation by Gallagher et al. (2002), while it is perhaps a factor of two higher than the HST G190/270H observation by Smith et al. (1995). As seen from Figure 6, earlier observations by IUE (Hutchings & Neff 1987) show that the continuum (λL_{λ}) levels of Mrk 231 at $1300\text{\AA} \sim 2.30, 3.20$, and $3.21 \times 10^{-12} \text{erg cm}^{-2} \text{s}^{-1}$ at three different epochs, and later on they are about 1.85 and $1.77 \times 10^{-12} \text{erg cm}^{-2} \text{s}^{-1}$ measured by the HST COS (Veilleux et al. 2013) and FOS (Gallagher et al. 2002). The probability for those observations to be consistent with a constant (or no variation) is 0.00013 according to the χ^2 -statistics, which suggests that the UV emission over the past several decades does vary, confirming the claim by Veilleux et al. (2013). However, these observations are not sufficient for investigating the expected (quasi-)periodical variations as done for the recently reported BBH candidate PG 1302-102 (Graham et al. 2015) because (1) the total number of the observations is small; and (2) the intervals between some of these observations are too large compared with the expected orbital period. Although there are more optical observations of Mrk 231, the number of observations at each individual band is limited and not sufficient for an analysis on the (quasi-)periodical variation.

Note that the periodical variation of the BBH candidate PG 1302-102 (Graham et al. 2015) has an amplitude of only ~ 0.14 magnitude (or $\sim 14\%$), which suggests that the amplitude of the expected periodical variations of some BBH-disk accretion systems may be small. Future intensive monitoring the UV continuum emission of Mrk 231 may reveal the periodical variation, which would confirm the BBH hypothesis and be useful to further constrain the dynamical interplay between the BBH and its surrounding accretion flow.

It has been shown that the polarization fraction of the optical-to-UV continuum of Mrk 231 depends on frequency and the peak of the polarization is around the wavelengths $\sim 3000\text{\AA}$ (Smith et al. 1995). This dependence is probably due to the scattering clouds distributed asymmetrically about the illuminating source (Smith et al. 1995). In the BBH

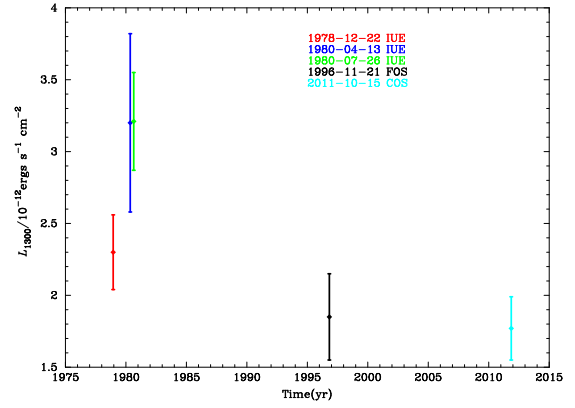


FIG. 6.— UV continuum flux at 1300\AA (L_{1300}) for Mrk 231 at different epochs. Different points are obtained from the UV spectra obtained by IUE and HST at different epochs as marked in the figure, smoothed over a wavelength range of 20\AA around 1300\AA at the rest frame. The bars associated with each point represent the $1\text{-}\sigma$ standard deviation of the measurement.

scenario, the blue photons around 3000\AA are mainly emitted from the inner edge of the circumbinary disk, where the disk may be puffed up because of the accumulation of accreting hot material there, which may lead to more significant scattering of those blue photons emitted from that region and thus a high polarization fraction; while those photons at the FUV and optical bands may experience less scattering as they are away from the inner edge of the circumbinary disk. This may explain the frequency dependence of the polarization fraction, qualitatively; Veilleux et al. (2013) and Leighly et al. (2014), likewise, also provided qualitative explanations on these polarization measurements in their competing models.

The standard accretion disk model adopted in the fitting is simple, and the torque due to the BBH on the outer disk is not considered. As shown in the Appendix, we adopt the model by Rafikov (2013) to fit the continuum, in which both the internal viscosity and the external torque by the BBH on the circumbinary disk are considered, and we find that there are no significant differences in the constraints on the model parameters.

According to the best fit, the infalling rate from the circumbinary disk to the inner disk(s) is smaller than the accretion rate of the circumbinary disk by a factor of ~ 30 . Currently it is not clear whether such a small infalling rate can be realized in BBH–disk accretion systems. For close BBH–disk accretion systems, a number of simulations and analyses suggested that the infalling rate into the gap or the central cavity is substantially smaller than the accretion rate at the outer boundary of the circumbinary disk because of the tidal barrier by the central BBH (e.g., the 1D simulations by Milosavljević & Phinney 2005, the 3D simulations by Hayasaki et al. 2007, or the simple arguments by Rafikov 2013). However, some recent simulations showed that the infalling rate may not be significantly suppressed by the tidal barrier (e.g., Noble et al. 2012; MacFadyen & Milosavljević 2008) and it may be even comparable to the accretion rate in the case with a single central MBH (Farris et al. 2014; Shi & Krolik 2015). Considering that all those simulations are quite idealized, it is also not clear whether the accretion onto the central BBH is really significantly suppressed or not. Future more realistic simulations may help to demonstrate whether the small infalling rate found for the BBH-disk accretion system in Mrk 231 is possible.

The spectral features of Mrk 231 were recently proposed

to be explained by either (1) a hybrid model with both a young star burst (for the UV continuum) and an obscured quasar (for the optical continuum) (see Leighly et al. 2014) or (2) an absorption model with extremely large dust reddening at the NUV band but small reddening at the FUV band (see Veilleux et al. 2013). In the first model, the FUV emission is dominated by the young star burst with an age of ~ 100 Myr and therefore would have no significant short time-scale variations, which appears inconsistent with the observations. Veilleux et al. (2013) also argued that the broad asymmetric Ly α line cannot be produced if the FUV emission is from an extended star burst. While in the second model, a small fraction of FUV emission is leaked through the obscuring material, and the UV variability will depend on the stability of the leaking holes. Future monitoring observations of Mrk 231 at the FUV and NUV bands, and simultaneous multi-wavelength observations will be helpful to confirm the BBH–disk accretion explanation and further constrain the orbital evolution of the BBH in the core of Mrk 231.

7. CONCLUSIONS

In this paper, we show that various unique features in the optical-to-UV spectrum and the intrinsic X-ray weakness of Mrk 231 can all be well explained, if a pair of SMBHs exists in the core of Mrk 231, with the masses of the primary and the secondary SMBHs as $\sim 1.5 \times 10^8 M_\odot$ and $4.5 \times 10^6 M_\odot$, respectively. The existence of a BBH in Mrk 231 is compatible with its disturbed morphology and tidal features, which indicates a merger event in the past. (Note that the secondary SMBH is rather low in mass; however, it should be able to sink down to the center because the stars initially associated with it enhance the dynamical friction Yu see 2002.) The semimajor axis of this BBH is ~ 590 AU, about 190 times of the Schwarzschild radius of the primary SMBH, and its orbital period is just ~ 1.2 year, relatively short among the few known BBH candidates (Valtonen et al. 2008; Graham et al. 2015), which makes it an ideal system to study the dynamics of BBH systems. Such a BBH emits gravitational wave on tens of nanohertz, and the change rate of its orbital period due to gravitational wave radiation is about 40 seconds per orbit.

This BBH might be a target for gravitational wave studies in future.

The orbit of such a BBH system decays on a timescale of a few times of 10^5 year due to gravitational wave radiation and the torque of the circumbinary disk (Haiman et al. 2009), which is not too small compared with the lifetime of quasars (a few times 10^7 to 10^8 year; see Yu & Tremaine 2002; Shankar et al. 2013; Yu & Lu 2008). The majority of quasars are believed to be triggered by mergers of galaxies and consequently involve mergers of SMBHs (Volonteri et al. 2003), and those BBH systems with mass ratio in the range of a few percent to 1 may lead to a notch in the optical-to-UV continuum emission if their semimajor axes are in the range of a few hundreds to about one thousands gravitational radii (Roedig et al. 2014), which correspond to orbital decay timescales of 10^5 – 10^6 year (Haiman et al. 2009). Therefore, the occurrence rate of active BBH systems, with deficits in the optical-to-UV emission, may be roughly a few thousandths to about one percent among quasars (Yan et al. 2014). Our analysis of Mrk 231 demonstrates the feasibility of finding BBH systems by searching for the deficits in the optical-to-UV emission among the spectra of quasars, a new method proposed by a number of authors (Farris et al. 2015; Gültekin & Miller 2012; Sesana et al. 2012; Yan et al. 2014), in addition to those current practices by searching for the kinematic and image signatures of BBHs among AGNs/quasars (Boroson & Lauer 2009; Valtonen et al. 2008; Graham et al. 2015; Liu et al. 2014; Gaskell 1996; Bogdanovic et al. 2008; Tsalmantza et al. 2011; Eracleous et al. 2012; Ju et al. 2013; Rodriguez et al. 2006; Popović 2012).

We thank Zheng Zheng for finding a typo in an earlier version of the paper. This work was supported in part by the National Natural Science Foundation of China under grant nos. 11273004 (Q.Y.), 11103029 (C.Y.), 11373031 and 11390372 (Y.L.), and the Strategic Priority Research Program “The Emergence of Cosmological Structures” of the Chinese Academy of Sciences, Grant No. XDB09000000 (Y.L.). X.D. is supported by the NSF grant AST-1413056.

APPENDIX

The structure of the circumbinary disk may be different from that of a standard thin disk, especially at the region close to the inner edge, since the torque raised by the central binary may lead to gas accumulation there. According to Rafikov (2013), the evolution of the circumbinary disk under the actions of both the internal viscosity and the external torque can be described by a simple equation

$$\frac{\partial \Sigma}{\partial t} = -\frac{1}{r} \frac{\partial}{\partial r} \left[\left(\frac{\partial l}{\partial r} \right)^{-1} \frac{\partial}{\partial r} \left(r^3 \nu \Sigma \frac{\partial \Omega}{\partial r} \right) + \frac{2 \Sigma \Lambda}{\Omega} \right]. \quad (1)$$

Here t is the evolution time, Λ is the external torque per unit mass of the disk due to the central BBH, Σ , ν , and r are the surface density, kinematic viscosity, and radius of the disk, respectively, and $l = \Omega(r)r^2$ is the specific angular momentum of gas material on a circular orbit with a radius r . At each radius, the accretion disk properties can be characterized by the viscous angular momentum flux

$$F_J \equiv -2\pi\nu\Sigma r^3 \frac{d\Omega}{dr} = 3\pi\nu\Sigma\Omega r^2, \quad (2)$$

where the last equality is valid for a near Keplerian disk with $\Omega \simeq (GM_\bullet/r^3)^{1/2}$ and $M_\bullet = M_{\bullet,p} + M_{\bullet,s}$.

Since Λ in equation (1) is significant only in a narrow annulus at the inner edge of the disk, we can assume that $\Lambda = 0$ outside of some radius r_Λ , which is not too different from r_{in} . Outside r_Λ , the disk evolves according to Equation (1) with $\Lambda = 0$. The solution of this equation can be obtained by the standard approach introduced in Lynden-Bell & Pringle (1974) Lynden-Bell (1974), if the inner boundary condition (IBC) is assumed to be torque free. However, the central BBH exerts a torque on the inner boundary of the circumbinary disk, which can be approximated by $F_J(r_{\text{in}}) \approx -dL_{\text{BBH}}/dt = -L_{\text{BBH}}v_{\text{BBH}}/2a_{\text{BBH}}$, where $L_{\text{BBH}} = qM_\bullet(GM_\bullet a_{\text{BBH}})^{1/2}/(1+q)^2$ is the orbital angular momentum of the BBH, and $v_{\text{BBH}} \equiv da_{\text{BBH}}/dt$ is the inspiralling

speed of the BBH. According to Rafikov (2013) Rafikov (2013), this IBC may be written as

$$\left. \frac{\partial F_J}{\partial l} \right|_{r=r_{\text{in}}} = \dot{M}(r_{\text{in}}) = \chi \dot{M}_{\infty}, \quad (3)$$

where χ is assumed to be a constant (≤ 1). By this setting, $\dot{M}(r_{\text{in}})$ can be substantially smaller than \dot{M}_{∞} , and disk material may gradually accumulate near the inner boundary if $\chi < 1$. We set the accretion rate at the outer boundary as \dot{M}_{∞} . A self-similar solution can be obtained for the evolution of the circumbinary disk once the initial separation of the BBH is given [i.e., $a_{\text{BBH}}(t=0) = a_{\text{BBH},0}$]. With the solution of $F_J(r, t)$, the effective temperature of the disk can be obtained as

$$T_{\text{eff}}(r, t) = \left[\frac{3}{8\pi} \frac{F_J(r, t)\Omega}{\sigma_B r^2} \right]^{1/4}. \quad (4)$$

By integrating the multi-color black body emission over the whole circumbinary disk, we obtain the continuum flux as

$$F_{\lambda, c} = \int_{r_{\text{in},c}}^{r_{\text{out},c}} \frac{2\pi r}{D_1^2} \frac{2hc^2 \cos i / \lambda^5}{\exp[hc/\lambda k_B T_{\text{eff}}(r)] - 1} dr. \quad (5)$$

Here D_1 is the luminosity distance of Mrk 231, h is the Planck constant, k_B is the Boltzmann constant, $r_{\text{in},c} = a_{\text{BBH}}(t)/(1+q) + R_H$, $r_{\text{out},c}$ is set to be $10^5 GM_{\bullet}/c^2$, and $a_{\text{BBH}}(t)$ is the semimajor axis of the BBH at time t . The evolution of $a_{\text{BBH}}(t)$ is controlled by

$$\frac{da_{\text{BBH}}}{dt} = -\frac{a_{\text{BBH}}}{t_{\text{GW}}} - \frac{a_{\text{BBH}}}{t_J}, \quad (6)$$

where $t_{\text{GW}} = [5(1+q)^2/64q](R_g/c)(a_{\text{BBH}}/R_g)^4$ is the gravitation wave radiation timescale Peters (1964), $R_g = GM_{\bullet}/c^2$ is the gravitational radius, and $t_J \equiv L_{\text{BBH}}/2F_J$ is the characteristic timescale for the BBH orbit shrinking due to the coupling to the circumbinary disk. If we adopt this model to describe the circumbinary disk and adopt the standard thin disk model to describe the mini-disk, we can also fit the continuum of Mrk 231 by the MCMC technique. Under this approach, $f_{\text{Edd},s} = \chi f_{\text{Edd},c}/q$. The best fit is shown in Figure 7, and the constraint on $a_{\text{BBH},0}$ and t are $355R_g$ and 2.1×10^4 year, respectively. Other best-fit parameters are $M_{\bullet} = 10^{8.2} M_{\odot}$, $f_{\text{Edd},c} = 0.4$, $q = 0.02$, $\chi = 0.04$ (corresponding to $f_{\text{Edd},s} = 0.7$), $a_{\text{BBH}} = 343R_g \sim 540$ AU (corresponding to $r_{\text{in},c} = 402R_g$, $f_{r,s} = 0.12$), and $E_{\text{B-V}} = 0.14$. These results are roughly consistent with those shown in Figure 3, which are obtained without considering the torque of the BBH on the inner boundary of the circumbinary disk.

The torque due to the outer circumbinary disk on the mini-disk around the secondary SMBH and the shock induced by the infall streams onto the mini-disk (Lodato et al. 2009; Kocsis et al. 2012; Farris et al. 2015; Roedig et al. 2014), which are omitted in this study, may also introduce some errors to the fitting. Although many simulations and analysis suggest a flux deficit in the continuum emission from a BBH-disk accretion system because of the gap (or hole) in the disk, including the one by Roedig et al. (2014) with consideration of the shock heating hot-spot on the inner mini-disk(s), one new simulation by Farris et al. (2015) suggested that there may be no strong flux deficit in the continuum emission of a BBH-disk accretion system by considering the emission from the infalling streams. However, only a specific case with a mass ratio of 1 is considered in Farris et al. (2015) and the stream emission therein is approximated as a thermal emission without considering inverse Compton scattering and radiative transfer. Therefore, their results might not be applicable to other cases and need to be improved (see the discussion in Farris et al. 2015). Roedig et al. (2014) argued that the shock induced by the infalling streams on the mini-disk(s) may enhance the X-ray emission at $\gtrsim 100$ keV, which does not affect the X-ray emission with energy significantly less than 100 keV and thus does not affect our estimate on the 2 – 10 keV emission.

REFERENCES

- Armus, L., Surace, J. A., Soifer, B. T., et al. 1994, *AJ*, 108, 76
 Artymowicz, P., & Lubow, S. H. 1996, *ApJ*, 467, L77-L80
 Begelman, M. C., Blandford, R. D., & Rees, M. J. 1980, *Nature*, 287, 307
 Bogdanovic, T., Smith, B. D., Sigurdsson, S., Eracleous, M. 2008, *ApJS*, 174, 455
 Boroson, T. A., & Lauer, T. R. 2009, *Nature*, 458, 53
 Branch, D., Leighly, K. M., Thomas, R. C., & Baron, E. 2002, *ApJ*, 578, L37
 Comerford, J. M., Pooley, D., Gerke, B. F., & Madejski, G. M. 2011, *ApJ*, 737, L19
 Cuadra, J., Armitage, P. J., Alexander, R. D., & Begelman, M. C. 2009, *MNRAS*, 393, 1423
 Dai, X., Kochanek, C. S., Chartas, G., Kozlowski, S., Morgan, C. W., Garmire, G., & Agol, E. 2010, *ApJ*, 708, 278
 D’Orazio, D. J., Haiman, Z., & MacFadyen, A. 2013, *MNRAS*, 436, 2997
 Eggleton, P. P. 1983, *ApJ*, 268, 368
 Eracleous, M., Boroson, T. A., Halpern, J. P., & Liu, J. 2012, *ApJS*, 201, 23
 Escala, A., Larson, R. B., Coppi, P. S., & Mardones, D. 2005, *ApJ*, 630, 152
 Esin, A. A., McClintock, J. E., & Narayan, R. 1997, *ApJ*, 489, 865
 Farris, B. D., Duffell, P., MacFadyen, A. I., & Haiman, Z. 2014, *ApJ*, 783, 134
 Farris, B. D., Duffell, P., MacFadyen, A. I., & Haiman, Z. 2015, *MNRAS*, 446, L36
 Ferland, G. J., et al. 2013, *Rev. Mex. de Astron. y Astrof.*, 49, 137
 Fu, H., Yan, L., Myers, A. D., et al. 2012, *ApJ*, 745, 67
 Gallagher, S. C., Brandt, W. N., Chartas, G., Garmire, G. P., & Sambruna, R. M. 2002, *ApJ*, 569, 655
 Gaskell, C. M. 1996, *ApJ*, 464, L107
 Goodrich, R. W., & Miller, J. S. 2005, *ApJ*, 448, L73
 Graham, M. J., Djorgovski, S. G., Stern, D., Glikman, E., Drake, A. J., Mahaball, A. A., Donalek, C., Larson, S., & Christensen, E. 2015, *Nature*, 518, 74
 Gültekin, K., & Miller, J. M. 2012, *ApJ*, 761, 90
 Haardt, F., & Maraschi, L. 1993, *ApJ*, 413, 507
 Haiman, Z., Kocsis, B., & Menou, K. 2009, *ApJ*, 700, 1952
 Hall, P. B., Anderson, S. F., Strauss, M. A., et al. 2002, *ApJS*, 141, 267
 Halpern, J. P., & Filippenko, A. V. 1988, *Nature*, 331, 46
 Hayasaki, K., Mineshige, S., & Sudou, H. 2007, *PASJ*, 59, 427
 Hayasaki, K., Mineshige, S., & Ho, L. C. A 2008, *ApJ*, 682, 1134
 Hopkins, P. F., Richards, G. T., & Hernquist, L. 2007, *ApJ*, 654, 731
 Hutchings, J. B., & Neff, S. G. 1987, *AJ*, 93, 14

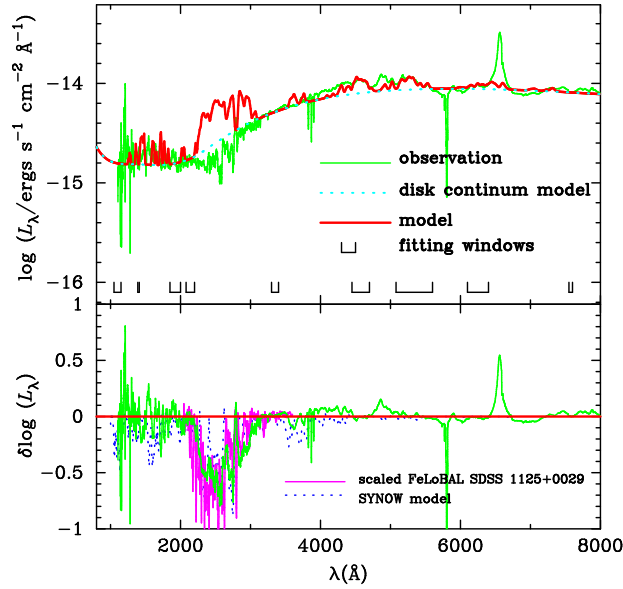


FIG. 7.— The optical-to-UV spectrum of Mrk231 and the model spectrum. Legend is similar to that for Fig. 3, except that the torque at the inner edge of the circumbinary disk is considered in the model fitting to the continuum emission.

- Ju, W., Greene, J. E., Rafikov, R. R., Bickerton, S. J., Badenes, C. 2013, *ApJ*, 777, 44
- Kocsis, B., Haiman, Z., & Loeb, A. 2012, *MNRAS*, 427, 2680
- Komossa, S., Burwitz, V., Hasinger, G., et al. 2003, *ApJ*, 582, L15
- Kormendy, J., & Ho, L. C. 2013, *ARA&A*, 51, 511
- Leighly, K. M., Terndrup, D. M., Baron, E., et al. 2014, *ApJ*, 788, 123
- Lipari, S., Colina, L., & Macchetto, F. 1994, *ApJ*, 427, 174
- Lin, D. N. C., Bodenheimer, P., & Richardson, D. C. 1996, *Nature*, 380, 606
- Liu, X., Greene, J. E., Shen, Y., & Strauss, M. A. 2010, *ApJ*, 715, L30
- Liu, X., Shen, Y., Bian, F., Loeb, A., & Tremaine, S. 2014, *ApJ*, 789, 140
- Lodato, G., Nayakshin, S., King, A. R., & Pringle, J. E. 2009, *MNRAS*, 398, 1392
- Lynden-Bell, D., & Pringle, J. E. 1974, *MNRAS*, 168, 603
- MacFadyen, A. I., & Milosavljević, M. 2008, *ApJ*, 672, 83
- Magorrian, J., Tremaine, S., Richstone, D., et al. 1998, *AJ*, 115, 2285
- Merritt, D., & Milosavljević, M. 2005, *Living Reviews in Relativity*, 8, 8
- Milosavljević, M., & Phinney, E. S. 2005, *ApJ*, 622, L93
- Noble, S. C., Mundim, B. C., Nakano, H., et al. 2012, *ApJ*, 755, 51
- Novikov, I. D., & Thorne, K. S. in *Black Holes*, ed. C. De Witt & B. De Witt (New York: Gordon & Breach), 343
- Osterbrock, D. E., & Ferland, G. J. 2006, *Astrophysics of gaseous nebulae and active galactic nuclei*, 2nd. ed. by D. E. Osterbrock and G. J. Ferland. Sausalito, CA: University Science Books.
- Pei, Y. C. 1992, *ApJ*, 395, 130
- Peters, P. C. 1964, *Phy. Rev.*, 136, 1224
- Phillips, M. M. 1977, *ApJ*, 215, 746
- Popović, L. Č. 2012, *New Astro Rev.*, 56, 74
- Quanz, S. P., Avenhaus, H., Buenzli, E., et al. 2013, *ApJ*, 766, L2
- Rafikov, R. R. 2013, *ApJ*, 774, 144
- Rodriguez, C., Taylor, G. B., Zavala, R. T., et al. 2006, *ApJ*, 646, 49
- Roedig, C., Sesana, A., Dotti, M., et al. 2012, *A&A*, 545, A127
- Roedig, C., Krolik, J. H., & Miller, M. C. 2014, *ApJ*, 785, 115
- Saez, C., Brandt, W. N., Gallagher, S. C., Bauer, F. E., & Garmire, G. P. 2012, *ApJ*, 759, 42
- Sesana, A., Roedig, C., Reynolds, M. T., & Dotti, M. 2012, *MNRAS*, 420, 860
- Shakura, N. I., & Sunyaev, R. A. 1973, *A&A*, 24, 337
- Shankar, F., Weinberg, D. H., Miralda-Escudé, J. 2013, *MNRAS*, 428, 421
- Shi, J.-M., & Krolik, J. H. 2015, arXiv:1503.05561
- Smith, P. S., Schmidt, G. D., Allen, R. G., & Angel, J. R. P. 1995, *ApJ*, 444, 146
- Teng, S. H., Brandt, W. N., Harrison, F. A., et al. 2014, *ApJ*, 785, 19
- Tsalmantza, P., Decarli, R., Dotti, M., & Hogg, D. W. 2011, *ApJ*, 738, 20
- Valtonen, M. J., Lehto, H. J., Nilsson, K., et al. 2008, *Nature*, 452, 851
- Veilleux, S., et al. 2013, *ApJ*, 764, 15
- Véron-Cetty, M.-P., Joly, M., & Véron, P. 2004, *A&A*, 417, 515
- Vestergaard, M., & Wilkes, B. J. 2001, *ApJS*, 134, 1
- Volonteri, M., Haardt, F., & Madau, P. 2003, *ApJ*, 582, 559
- Yan, C.-S., Lu, Y., Yu, Q., Mao, S., & Wambsganss, J. 2014, *ApJ*, 784, 100
- Yu, Q. 2002, *MNRAS*, 331, 935
- Yu, Q., & Lu, Y. 2008, *ApJ*, 689, 732
- Yu, Q., & Tremaine, S. 2002, *MNRAS*, 335, 965
- Zheng, W., Kriss, G. A., Telfer, R. C., Grimes, J. P., & Davidsen, A. F. 1997, *ApJ*, 475, 469